International Journal of Engineering

Journal Homepage: www.ije.ir

Evaluation of Linear Permanent Magnet Vernier Machine Topologies for Wave Energy Converters

N. Arish[a], F. Marignetti[*b]

[a] Faculty of Electrical and Computer Engineering, Semnan University, Semnan, Iran
[b] Department of Electrical and Information Engineering the University of Cassino and South Lazio, Cassino, Italy

PAPER INFO

Paper history:
Received 29 September 2020
Received in revised form 26 November 2020
Accepted 09 December 2020

Keywords:
Wave Energy
Energy Converter
Permanent Magnet Shape
Vernier Machine
Halbach Array
Linear Machine
Finite Element Method

ABSTRACT

Today, the importance of using vernier machines in wave energy converters has increased because of its simple structure and ability to generate a lot of thrust force at low speeds due to the magnetic gear effect. The linear vernier permanent magnet machine has been designed in various structures. Proper design and selection of the main parameters of the machine will improve performance and increase the efficiency of the linear vernier machine. One of these parameters is the shape of the permanent magnets and how they are magnetically oriented. The novelty of this paper is the reduction of leakage flux, achieved by changing the shape and orientation of the permanent magnet. Three types of linear permanent magnet vernier machines with different permanent magnet structures and orientation, including V-shape, Halbach array and consequent-pole are presented. The considered machines have been compared to each other and to the existing machine in terms of airgap flux density, back EMF, PM flux, Inductance, thrust force, detent force, loss, efficiency, power factor, flux density and flux line, using the finite element method in the same conditions and with the same volume of permanent magnets. The results show that the magnetic orientation and shape of the permanent magnet have a considerable effect on the leakage flux, and all the proposed models have a lower leakage flux and better performance compared to the existing model.

doi: *10.5829/ije.2021.34.02b.12*

1. INTRODUCTION

The belief that non-renewable energies will run out one day has always been the best motivation for researchers and scientists to think about how to take advantage of clean energy as well as replacing non-renewable energy [1, 2]. Wave energy and wind energy is one of the most important renewable energies due to its relatively high energy density and high predictability, which requires electric converters to exploit it [3, 4]. Linear Permanent Magnet Vernier Machine (LPMVM) is one of these converters, which has been used widely in several structures and operated base on the magnetic gear effect [5]. Magnetic gear effect is a phenomenon that magnetic field in the air gap with a small movement of translator changes remarkably, which provides the ability to produce high thrust force at low speeds. The reason for this feature is the existence of a large number of magnetic pole pairs. Each structure of LPMVM has advantages and disadvantages that are used based on constraints, location and circumstances. The Vernier machine, in addition to advantages such as high torque production at low speeds and a robust and simple structure, has one main drawback. High leakage flux due to the presence of several pairs of magnetic poles causes low power factor (PF) that is an inherent fundamental weakness among all the vernier machines [6]. Over time, various methods have been proposed to improve the PF and performance of LPMVM, each one reducing leakage flux. One of the most important factors influencing leakage flux and

*Corresponding Author Email: marignetti@unicas.it (F. Marignetti)

Please cite this article as: N. Arish, F. Marignetti, Evaluation of Linear Permanent Magnet Vernier Machine Topologies for Wave Energy Converters, International Journal of Engineering, Transactions B: Applications Vol. 34, No. 02, (2021) 403-413

power factor is the structure of magnets and their magnetic orientation [7]. Shi et al. [8] and Almoraya et al. [9], changing the shape and orientation of the permanent magnets from simple to skew, were able to diminish leakage flux in the air gap and increase the electromagnetic performance of the proposed machines. Huo et al. [10] by adding smaller magnets with a horizontal magnetic orientation to larger magnets with vertical magnetic orientation, created an integrated Halbach array that reduces leakage flux and increases machine efficiency. Zhao et al. [11] and shi et al. [12] improved thrust force, flux density and back EMF in the presented machines by dividing the magnet into smaller magnets in different magnetic directions and converting the magnet with a simple array to Halbach array. Nematsaberi et al. [13], by using the spoke array permanent magnet instead of a simple permanent magnet and adding non-magnetic material decreased the leakage flux remarkably which raised the thrust force and PF. Arish et al. [14] have improved the performance of the proposed machine by reducing leakage flux and increasing generation of the magnetic field by hybrid structure and the simultaneous use of two different permanent magnet structures, skew and Halbach [15]. Khaliq et al. [16] have reduced the leakage flux in the proposed machine by using a spoke array permanent magnet in the dual stator structure. Arish et al. [17] by using high-temperature superconductor (HTS) material as bulk between the slot of stator reduced leakage flux and improved electromagnetic performance of the proposed machine. Almoraya et al. [18] by changing the magnetic circuit, not only reduced the volume of PM but also increased the performance of the proposed machine. The purpose and novelty of this paper are to improve the performance of the existing LPMVM and reducing leakage flux by changing the magnetic orientation and shape of the permanent magnets. Therefore, three models are presented with the same volume of PM, but different geometry and orientation. All PMs are located on the stator as a Halbach array, V-shape, Consequent-pole, and base-line (existing) which are shown in Figure 1. The structure of this article is as follows: all the models are examined in section 2. The main function of the presented machines is analyzed section 3. The electromagnetic characteristics in all models are analyzed by FEM and compared with each other in section 4, and finally, the conclusion is given in the last part. The research methodology is also summarized in Figure 2 as a flowchart.

2. MACHINE STRUCTURE

The operation of all the proposed models is in the form of wave energy converters installed on shallow shores so that the stator is fixed on the shore and there is a mechanical arm in the water that transmits the wave energy to the translator and moves it which is shown in Figure 3. The energy of wave with variable speeds is captured by a mechanical arm and changed to the standard range by mechanical gear. A power electronic converter is used for the network connection of the wave energy converter which links the voltage of the wave energy converter with a changing frequency and amplitude to the network with a fixed frequency and amplitude, because of the irregular movement of continuously varying speed. All models have been made of laminated iron translator and stator which 3-phase concentrated winding and NdFeB rare earth magnet are located on the stator. All models have a total of six coils which each phase has two coils. The stator contains six major teeth in which each of them is divided into smaller teeth which are known as flux modulation teeth. All models have been designed at a constant permanent span and the same condition such as materials, geometry, speed, armature current, number of turn per coil and frequency. The key design parameters of the Baseline model are depicted in Figure 4 and written in Table 1.

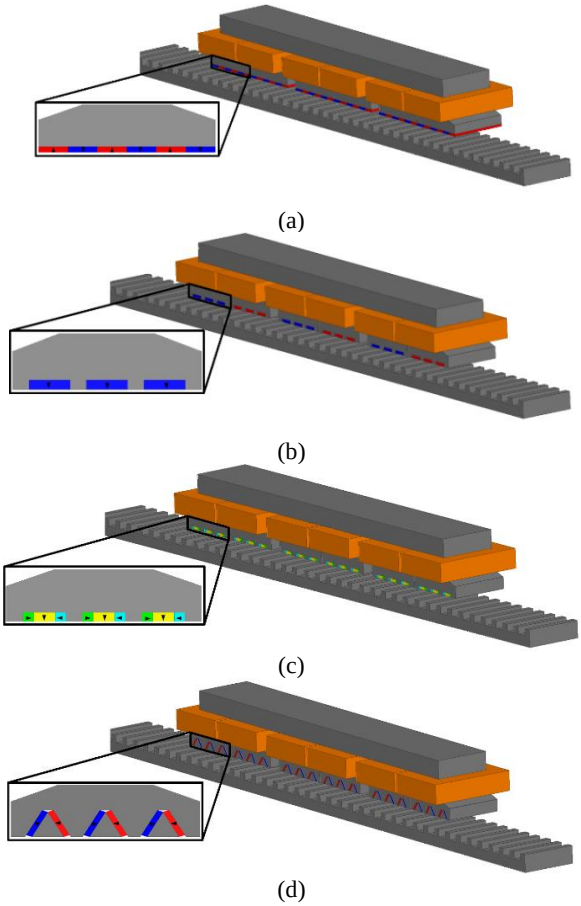

Figure 1. Machines structure. (a) Baseline model (existing), (b) Consequent-pole model, (c) Halbach model, (d) V-shape model

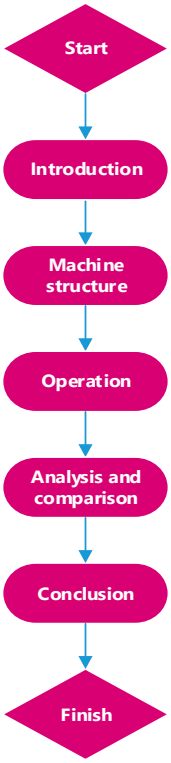

Figure 2. The flowchart of the research methodology

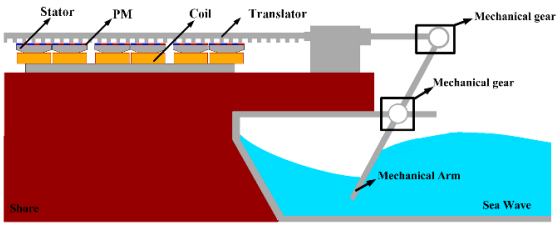

Figure 3. Operation of the linear permanent magnet vernier machine as a wave energy converter

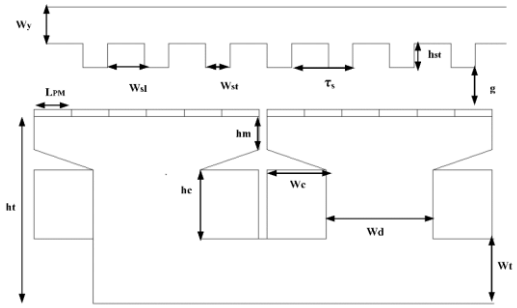

Figure 4. The key design parameters of the Baseline model

2. 1. Baseline Model The Baseline model is known as a simple and rigid structure with high thrust force and force density [19]. In this structure, permanent magnets are mounted on the surface of the stator as tandem and without any space. All PMs are magnetized in two vertical magnetic orientations (upward and downward) one after another.

TABLE 1. The key design parameters of the Baseline model

Items	Unit	Proposed machine
Rate current	A	7
Speed	m/s	1.5
Thickness of PM	mm	3
g	mm	2
w_y	mm	10
w_t	mm	16
w_{st}	mm	6
w_{sl}	mm	9
h_{st}	mm	6
h_m	mm	8.25
h_t	mm	46.25
w_c	mm	14
h_c	mm	17
τ_s	mm	15
l_{PM}	mm	9
w_d	mm	26

2. 2. Consequent-pole Model The Consequent-pole model is as same as the Baseline model in terms of structure and operation [20]. The only difference between them is the thickness of PMs, which, in the Consequent-pole pole model, is twice the Baseline model. Also, orientation in the major teeth is in one direction and changes by every major tooth. So that, if the magnetic orientation of all magnets on the first major teeth is upward, the magnetic orientation of all magnets in the consequent major teeth is downward.

2. 3. Halbach Model In this structure, permanent magnets are divided into three segments in which a vertical magnetized magnet is located between two horizontal magnetized magnets. The middle part generates the main flux, while two other parts operate as a flux barrier and reduce leakage flux at the edge of the magnets. Thickness and width of the Halbach array PMs have a remarkable effect on the performance of the machine and, with the correct selection of the width of segments based on Equations (1) and (2), both back EMF and PM flux can be sinusoidal and symmetrical [11].

$$w_v + 2w_h < \tau_s \quad (1)$$

$$w_h \leq w_v \quad (2)$$

2. 4. V-Shape Model In this structure, simple permanent magnets are divided into two segments as V-shape which are magnetized in two different horizontal orientations that guide the flux into the teeth of the stator and the translator. Skewing of permanent magnet reduces leakage flux, detent force, and ripple force [21].

3. OPERATION

The pole pitch and teeth pitch of the Vernier machine play a prominent role in its operation. The pole pitch of the translator is given by Rostami et al. [22]:

$$\tau_s = \frac{n_s}{l_a} \tag{3}$$

where n_s and l_a are the active teeth number of the stator and active length of the linear permanent magnet vernier machine, respectively. The frequency of a linear permanent magnet Vernier machine is related to the translator's speed (v) and translator pole pitch (τ_s) , as:

$$f = \frac{v}{\tau_s} \tag{4}$$

The relationship between the number of pole pairs of the air gap (P_w) and the permanent magnet field (P_{pm}) and stator teeth (P_s) can be expressed as follows :

$$P_w = \frac{P_s - P_{pm}}{P_s} \tag{5}$$

The gear ratio (*Gr*) has been known as the ratio of the number of stator's teeth and pole pairs of the air gap [12]:

$$G_r = \frac{P_s}{P_w} \tag{6}$$

The speed of the magnetic field generated by the permanent magnet is directly related to the gear ratio and, increasing gear ratio, the speed of the magnetic field increases. This expresses that the speed of magnetic field (V_{eff}) is much larger than the speed of the translator:

$$G_r = \frac{P_s}{P_w} = \frac{V_{eff}}{v} \tag{7}$$

Magnetic gear effect in Vernier machine is a unique feature, and a considerable change in the magnetic field causes all models to be capable of generating high thrust force at low-speed with small displacement. The magnetic gear effect operates at one pole pitch in four main steps. In all models, when the permanent magnet is aligned with the translator's teeth, which is defined as the initial position (X=0), linkage flux is at the maximum value. By moving the translator at the right hand as a quarter of the translator's pole pitch (X= 1/4 τ_s), the linkage flux drops to zero. In the next positions (X= 1/2 τ_s) and (X= 3/4 τ_s), the flux linkage reaches the minimum value and zero, respectively. This cycle is repeated by moving the translator for all models. The effect of the magnetic gear ratio has been depicted for the Baseline model in Figure 5 for four main positions. As can be seen, the low change of the mechanical position of the translator leads to a significant change of linkage flux. Waveforms of back EMF and PM flux have been depicted in four main positions for phase B in Figure 6.

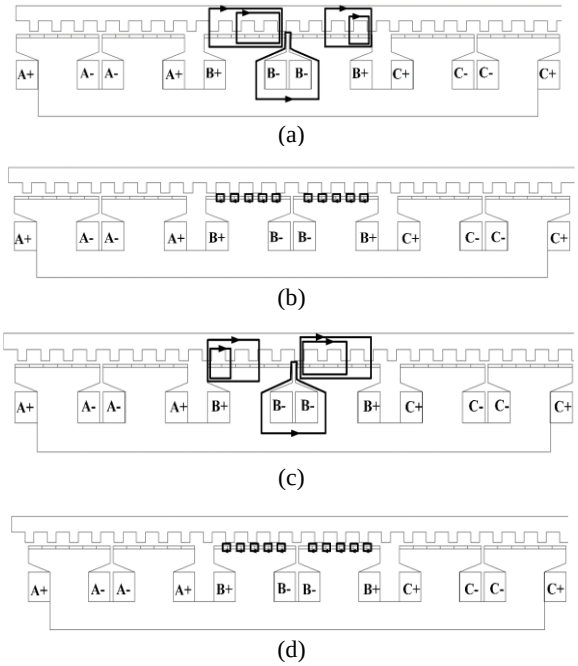

Figure 5. The effect of the magnetic gear ratio in four main positions

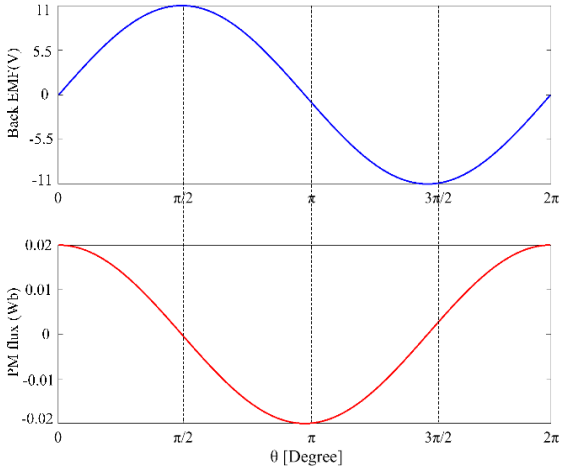

Figure 6. Waveforms of back EMF and PM flux in four main positions for phase B

4. ANALYSIS AND COMPARISON

Basically, the analysis of electric machines in two-dimensional and three-dimensional space is done by the FEM by solving the partial differential equations governing meshing. There are different ways to solve these equations that eventually all come to the same answer [23, 24].

To increase the accuracy of the analysis, the number of mesh elements can be increased and the mesh size can be minimized. These actions may result in an increase in the computation time, although with a little improvement of the results accuracy. Therefore, in order to increase the accuracy of the results and decrease the computation time, in some areas like the air gap, where the flux lines change more, the size of the mesh can be selectively decreased and the number of mesh elements can be raised. To find the best number of meshes, analyses have been done for the baseline model with the various number of the mesh by step of 2000 meshes ie: (4000, 6000, 8000, 10000, 12000, 14000, 16000 and 18000). For a better comprehension, all electromagnetic characteristics of the baseline model have been written in Table 2 for various range of mesh. It is evident that 12000 number of meshes which were created on the surface of the electrical machine is the best step for analyses, because after that not only the results don't change considerably but also it is time-consuming. The meshing method for the Baseline model is shown in Figure 7. For an accurate and fair comparison, performance analysis of all models has been carried out at the transient (full-load) and magnetostatic (no-load) states at the same geometry, materials, speed, current, frequency, turn per coil, magnet pitch and volume. The only variable are the shape and orientation of PM. All analyses have been done in terms of back EMF, PM flux, inductance, thrust force, loss, PF, efficiency and detent force. The conditions of sea wave are very different and consequently, the translator's speed changes continually during its performance. All analyses for all models have been done for a wide range of speeds (0.5 to 3 m/s). Results of electromagnetic analyses of all models respected to the speed have been depicted in Figure. 8. As can be seen, speed of translator does not have considerable impact on the inductance and inductance in all speeds is constant. On the other hand, by increasing speed of the translator, PM flux and back EFM increased too.

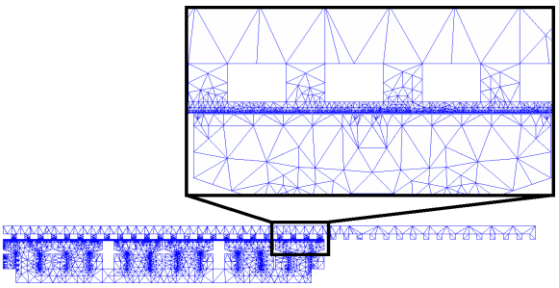

Figure 7. The meshing method of the Baseline model

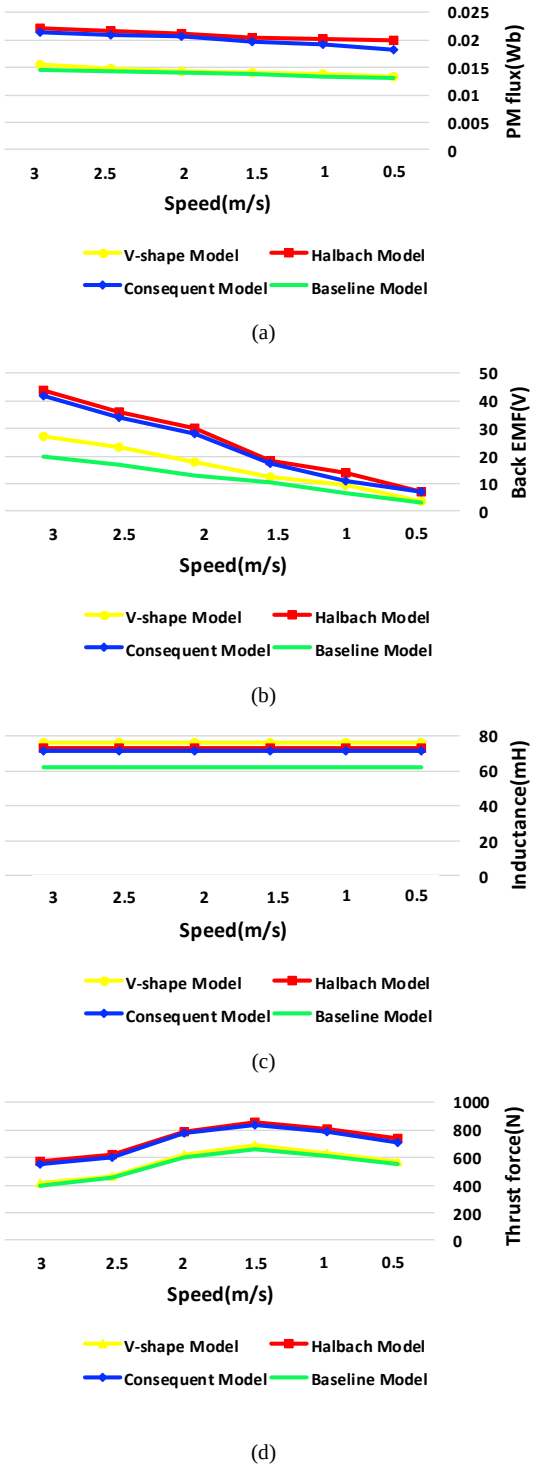

Figure 8. Electromagnetic charictristics of all models respect to speed. a)PM flux, b) Back EMF, c) Inductance, d) Thrust force

TABLE 2. The electromagnetic characteristic of baseline model for various number of meshes

Number of meshes	PM flux (Wb)	Back EMF (V)	Inductance (mH)	Detent force (N)	Thrust force (N)
4000	0.0135	10.4	61.3	39	680
6000	0.0136	10.45	61.5	39.8	684
8000	0.0137	10.5	61.9	40.3	686
10000	0.0137.5	10.55	62.1	40.6	688
12000	0.0138	10.6	62.21	41	690
14000	0.01383	10.63	62.26	41.1	691
16000	0.013835	10.68	62.28	41.3	691.2
18000	0.013839	10.69	62.29	41.5	691.5

However, by raising the speed of translator, thrust force in all models at first increases and then reduces. It shows that linear vernier machine is able to generate high thrust force at the low speed (0.5 -1.5 m/s). It should be noted that by increasing the speed of translator, ripple of thrust force increases and waveforms of PM flux and back EMF lose their pure sine. Following that, best performance of all models is at the range speed of (0.5 to 1.5 m/s).

4. 1. No-load Performance Analysis No-load analysis has been done at the open circuit position while just PM generate a magnetic field. Analysis of the air gap flux density, PM flux, back EMF, detent force, and flux line distribution have been carried out in this state. Since in all models, magnet volume and magnet span are constant, the flux line generated by PMs is also constant. The reduction of leakage flux increases the magnetic field in the core and improves electrical machine performance. Figure 9 shows flux line distribution for all models which according to this figure, the flux path of flux linkage and leakage flux are at the same position (x=0). As can be seen, leakage flux in the air gap is various in all models and is higher in the Baseline model compared to other models. It is evident that the shape and magnetic orientation of the permanent magnet have a considerable impact on the leakage flux. Figure 10 depicts the air gap flux density of all models. The interaction of teeth of the translator and magnetic field generated by PM results in magnetic flux in the air-gap. Peak values of air-gap flux density for the Baseline model, Consequent-pole model, Halbach model and V-shape model are 0.510 T, 523 T, 0.543 T and 0.310 T, respectively. Halbach array and Consequent-pole model have higher air-gap flux density compared to other models indicating that these two models have the lowest flux leakage. The back EMF is a derivative of PM flux over time, which means that these parameters are interdependent and change accordingly. The reduction of leakage flux increases the effective flux and magnetic field which accordingly increases the PM flux and then back EMF.

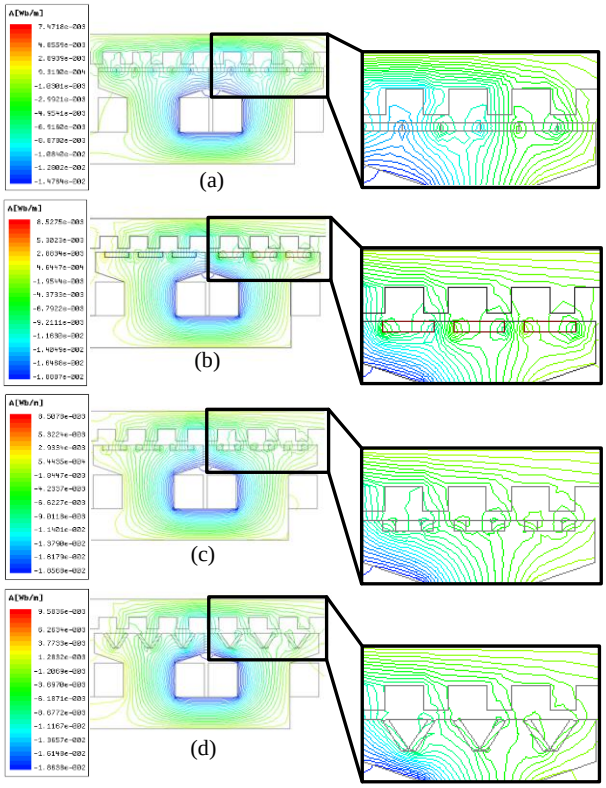

Figure 9. Flux line distribution for all models. (a) Baseline model, (b) Consequent-pole model, (c) Halbach model, (d) V-shape model

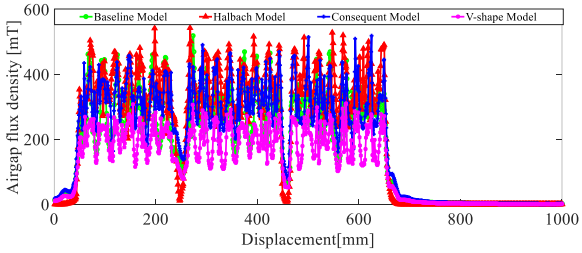

Figure 10. Comparison of air gap flux density

By changing the flux path in the core of the machine, the value and the orientation of the PM flux in the winding will change simultaneously, which makes inducing the back-EMF [11].

$$EMF = \frac{d\psi_m}{dt} = \frac{d\psi_m}{dx}.\frac{dx}{dt} = \frac{d\psi_m}{dx}.v \quad (8)$$

where, x, v and ψ are translator movement, translator speed and PM flux. Figures 11 and 12 show back EMF and PM flux for all models at the same speed and condition. It is evident that Halbch and Consequent-pole models generate higher PM flux and back EMF compared to other models, due to the low leakage flux. RMS values of PM flux for Baseline model, Consequent-pole model, Halbach model and V-shape model are 0.0138 Wb, 0.0196 Wb, 0.0204 Wb and 0.0141 Wb, respectively. Also, maximum values of back EMF for Baseline model, Consequent-pole model, Halbach model and V-shape model are 10.6 V, 17.5 V, 18.4 V and 12.2 V, respectively. In the Halbach model, the flux is finely distributed in the air gap in comparison to the near-constant flux density above the inset magnet, because the flux spreads uniformly through the pole piece, so the waveform in this model is more sinusoidal than other models. Detent force is a detrimental factor in the performance of electric machines, causing vibration and noise and reducing machine efficiency [25, 26]. Detent force consists of two main factors, slot effect and end effect. In linear vernier machines, end effect has a great impact on the detent force. The detent force for all models is shown in Figure 13. The peak 2 peak values of the detent force for Baseline model, Consequent-pole model, Halbach model and V-shape model are 41 N, 53 N, 17 N and 28 N, respectively.

4. 2. Full-load Performance Analysis Full-load analysis has been done while winding and PM generate magnetic field simultaneously. Analysis of flux density distribution, inductance, thrust force, PF, loss and efficiency has been carried out in this state. The flux-density distribution for all models is depicted in Figure 14. As can be seen, magnetic field in all models in the teeth of the stator and translator is higher than in other parts of the machine.The maximum value of the magnetic field is in the standard range and lower than *2T*, which clarifies that all machines operate properly and are not saturated. Inductance for each phase in Vernier machine are obtained at the full load state. For example, for phase-A, self-inductance can be calculated when DC current (i_a=7A) is applied to phase-A, while other phases are at the no-load state (Ib=Ic=0) [25].

$$L_{aa} = \frac{\phi_a(I_b = I_c = 0, I_a = I) - \phi_a(I_a = I_b = I_c = 0)}{I} \quad (9)$$

Figure 15 depicts the Inductance for all models. The average values of inductance for Baseline model, Consequent-pole model, Halbach model and V-shape model are 62.21 mH, 72.67 mH, 72.85 mH and 76.38 mH, respectively. The equivalent circuit of phase-A has been drawn in Figure 16. The terminal voltage for phase-A for the vernier machine can be obtained by Equation (10):

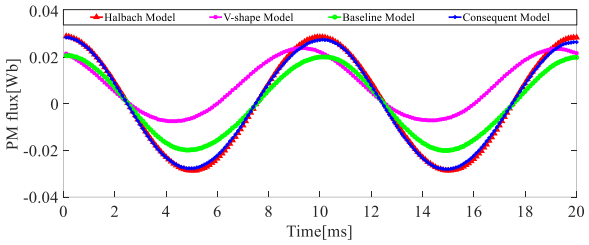

Figure 11. Comparison of PM flux

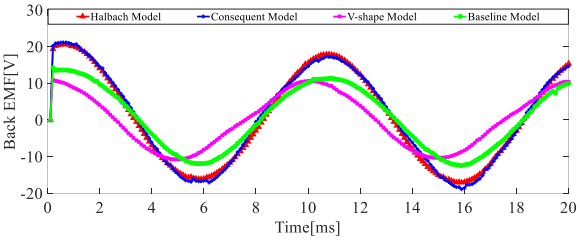

Figure 12. Comparison of back EMF

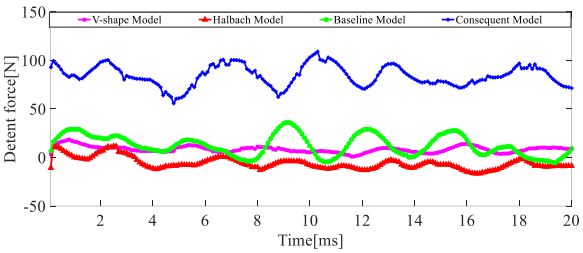

Figure 13. Comparison of detent force

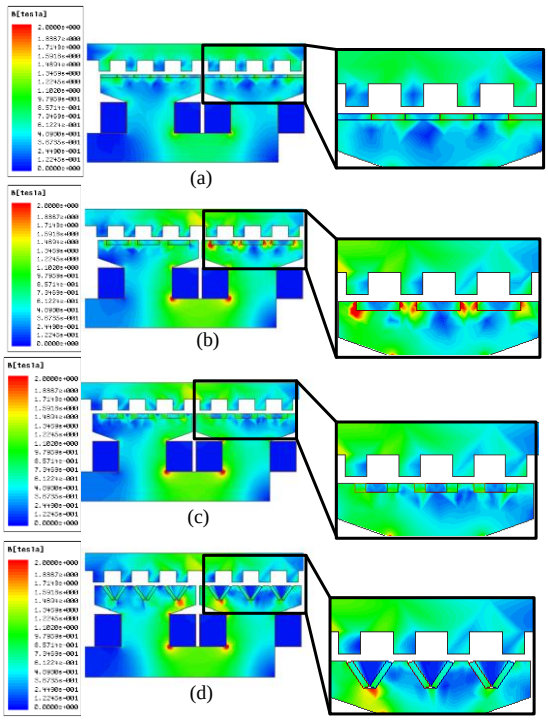

Figure 14. Flux density distribution for all models. (a) Base line model, (b) Consequent-pole model, (c) Halbach model, (d) V-shape model

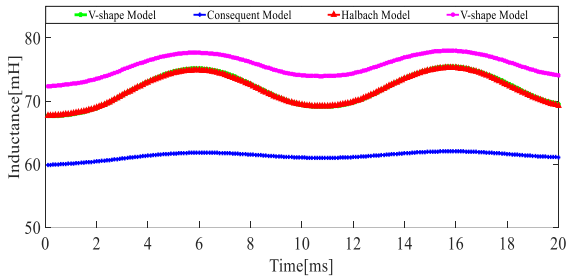

Figure 15. Comparison of inductance

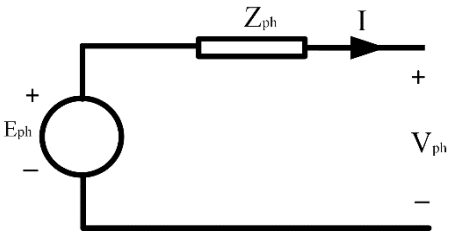

Figure 16. The equivalent circuit of phase-A

$$V_{ph} = R_a I_a + L_S \frac{di_a}{dt} + E_{ph} \quad (10)$$

The terminal voltage of phase-A is obtained by adding the no-load back EMF with voltage drop of the armature resistance and armature inductance.

The power factor in linear Vernier permanent magnet machine is low as shown in the phasor diagram. The phasor diagram has been depicted in Figure 17 by neglecting stator resistance. Because of the insignificant internal resistance, the voltage drop can be neglected for simple computation [13].

$$\cos\theta = \frac{E_{ph}}{V_{ph}} \approx \frac{E_{ph}}{\sqrt{E_{ph}^2 + (I_q X_q)^2}} \quad (11)$$

where, E_{ph} is no-load back EMF, V_{ph} is the terminal voltage, Iq is the q-axis current and Xq is the q-axis inductance. For constant terminal voltage, by diminishing current and average of inductance, PF can be improved. Figure 18 shows the variation of thrust force for all models with respect to the current. The Halbach model has the best overload capability than the Consequent-pole model because of the magnetic orientation. In fact, the saturation range in the halbach PM is larger than using a simple PMs disposition. Increasing the current value from 1 A to 7 A, the thrust force increases dramatically and, increasing further, all models saturate and the thrust force does not change considerably, which clarifies that 7 A is the best selection for the current. The thrust force for all models is in Figure 19. The average values of the thrust force for Baseline model, Consequent-pole model, Halbach model and V-shape model are 690 N, 860 N, 840 N and 660 N, respectively. The ratio of the peak-to-peak value of the thrust force to the average of the thrust force is defined as the ripple force. This index may be used to reduce the ripple force noise and diminish vibrations, so to improve performances of the electrical machine:

$$Ripple - Force = \frac{Force_{\max} - Force_{\min}}{Force_{avg}} \times 100 \quad (12)$$

Ripple force is caused by several reasons: asymmetrical three-phase windings and high amount of detent force, higher harmonics in the waveform of back-EMF and non-sinusoidal stator current waveforms and air gap flux-density. In order to reduce the value ripple force using concentrated winding, skewing slot of the translator and PM, and selecting suitable magnetic gear ratio are effective solutions [26-28]. The ripple force for Baseline model, Consequent-pole model, Halbach model and V-shape model is 24, 16, 14, 29%, respectively. In order to determine the cost-effectiveness in terms of the generation of thrust force for all models, the average thrust density of the machines can be calculated according to literature [29, 30]. Where, F,

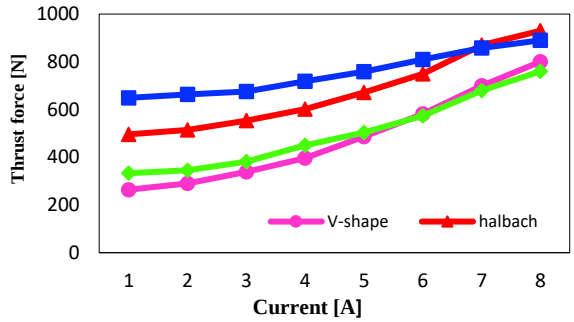

Figure 18. Thrust force of all models respect to the current

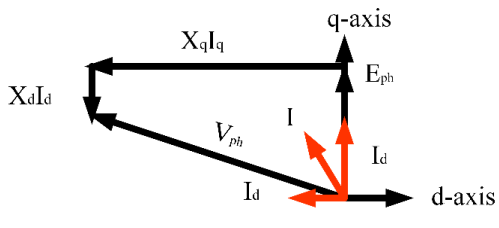

Figure 17. Phasor diagram

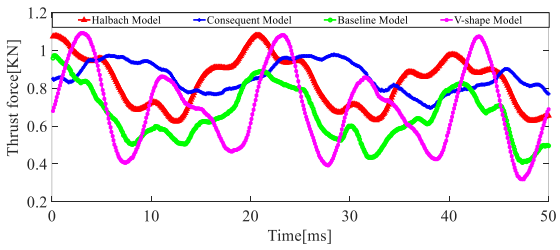

Figure 19. Thrust force waveforms for all models at 7 A

V and F_d are the average of thrust force, active volume of machine and force density, respectively. The values of force density for Baseline model, Consequent-pole model, Halbach model and V-shape model are 34055 N/m^3, 42446 N/m^3, 41458 N/m^3 and 32574 N/m^3, respectively. The shear stress for all models can be obtained by the following formula [9]:

$$F_d = \frac{F}{V} \tag{13}$$

$$\sigma = \frac{F}{A_{airgap}} \tag{14}$$

where σ is the shear stress and A_{airgap} is the air gap area. The values of shear stress for Halbach array, V-shape, Consequent-pole and Bbase-line are 953 KN/m^2, 1187 KN/m^2, 1160 KN/m^2 and 911 KN/m^2, respectively. The PF is one of the most critical parameters in Vernier machines, because it is normally low due to high leakage flux. PF can be calculated as follows [6]:

$$PF = \frac{1}{\sqrt{\frac{LI}{\phi}+1}} \tag{15}$$

where, ϕ, I and L are the PM flux, phase current and inductance in the LPMVM, respectively. Clearly, reducing inductance and phase current and increasing PM flux, the power factor will increase. PF for Baseline model, Consequent-pole model, Halbach model and V-shape model is 0.21 , 0.23, 0.22, 0.19, respectively. Core losses are created by the alternating magnetic field in the iron parts. The major components of the core losses are the hysteresis and the eddy current losses. Eddy current loss is created as a coil is wrapped around a core and an alternating AC supply is applied. The flux produced in the coil is alternating as long as the supply to the coil is alternating. Altering the flux by the core causes an induced emf inside the core, based on the Faraday's law of electromagnetic induction. The current starts to flow in the core by the emf induction. Hysteresis loss is generated by the magnetization and demagnetization of the core caused by the flow of the current in the forward and reverse directions, that laminating the core can decrease the eddy current losses and hysteresis losses.

The total loss and efficiency for all models at fixed current density and coil area are calculated and compared. Total loss for the Baseline model, Consequent-pole model, Halbach model and V-shape model are 21 W, 20.7 W, 20.5 W, 20.3 W, respectively. Efficiency for all models can be calculated as follows:

$$\eta = \frac{P_{out} - loss}{P_{out}} \times 100 \tag{16}$$

Efficiency for the Baseline model, Consequent model, Halbach model and V-shape model are 75, 86, 85 and 80%, respectively. The main electromagnetic parameters of all models have been written in Table 3. Also, For better comprehension, the performance of similar structures of the vernier machine which were explained in the introduction has been compared to all the presented models in Table 4.

TABLE 3. The comparison of electromagnetic characteristics

	Unit	Baseline Model	Consequent-pole Model	Halbach Model	V-shape Model
Airgap flux	T	0.510	0.523	0.543	0.310
PM flux	Wb	0.0138	0.0196	0.0204	0.0141
Back EMF	V	10.6	17.5	18.4	12.2
Inductance	mH	62.21	72.67	72.85	76.38
Detent force	N	41	53	17	28
Thrust force	N	690	860	840	660
Ripple force	%	24	16	14	29
Force density	N/m^3	34055	42446	41458	32574
Shear stress	KN/m^2	953	1187	1160	911
Loss	W	21	20	20.5	20.3
Efficiency	%	75	86	85	80
PF	-	0.21	0.22	0.23	0.19

TABLE 4. Performance comparison of similar structures

	PM flux (RMS)	Induced voltage (Max)	Inductance (Avg)	Thrust force (Avg)	PF
Unit	Wb	V	mH	N	
A model [6]	0.036	9.4	-	599	0.74
B model [7]	-	59	16.3	818	0.65
C model [8]	-	40	-	2332	0.51
D model [9]	0.057	65	-	1087	-
E model [10]	-	21.4	-	1650	0.47
F model [11]	0.18	86	-	2200	0.28
G model [12]	0.081	23	18.1	1860	-
H model [13]	0.049	34	16	2300	-
I model [14]	0.49	167	-	4950	-
J model [15]	0.141	60	43	1860	-

Basline model	0.0138	10.6	62.21	690	0.21
Halbach model	0.0204	18.4	72.85	840	0.23
V-Shape model	0.0141	12.2	76.38	660	0.19
Consequent-pole model	0.0196	17.5	76.67	860	0.22

5. CONCLUSION

In this article, three structures of LPMVM have been proposed. All structures have a concentrated winding mounted on the stator and PM on the translator as Halbach array, V-shape array, and Consequent-pole array. The purpose of this paper is to analyze the effect of magnetic orientation and shape of the PM on the flux leakage and performance of LPMVM, operating as a wave energy converter. For a fair comparison, all models are compared to each other using the FEM method using the same condition and geometry in terms of airgap flux density, back EMF, PM flux, Inductance, thrust force, detent force, loss, efficiency, power factor, flux density, and flux lines. The highest value of the air gap flux density belongs to the Halbach model, which indicates that this model has the lowest flux leakage. Also, the maximum RMS of the PM flux, power factor, and peak values of the back EMF belongs to the Halbach model. Moreover, the lowest peak-to-peak value of the detent force belongs to the Halbach model which shows that the Halbach model has the lowest ripple force. Minimum and maximum of total loss and efficiency belong to Consequent-pole model, respectively. Also, the maximum value of force density, shear stress, and average thrust force belongs to the Consequent-pole model. It should be noted that the minimum of the average value of the inductance belongs to the Halbach model and the V-shape model. The results show that changing the shape and orientation of PM has a considerable effect on the performance of LPMVM which is used for wave energy converters.

6. REFERENCES

1. Kibaara, Samuel Kariuki, et al. “Comparative Analysis of Implementation of Solar PV Systems Using the Advanced SPECA Modelling Tool and HOMER Software: Kenyan Scenario.” ***HighTech and Innovation Journal***, Vol. 1, No. 1, (2020), doi.10.28991/hij-2020-01-01-02.
2. Aminoroayaie Yamini O, Mousavi SH, Kavianpour MR, Movahedi A "Numerical modeling of sediment scouring phenomenon around the offshore wind turbine pile in marine environment". ***Environmental Earth Sciences***, Vol. 77, No. 23, (2018) doi.org/10.1007/s12665-018-7967-4.
3. Ha, K., "Innovative Blade Trailing Edge Flap Design Concept using Flexible Torsion Bar and Worm Drive". ***HighTech Innovation Journal,*** Vol. 1, No. 3, (2020). doi.org/10.28991/hij-2020-01-03-01.
4. Yamini, O. A., et al. “Wave Run-up and Rundown on ACB Mats under Granular and Geotextile Filters’ Condition.” ***Marine Georesources and Geotechnology***, Vol. 36, No. 8, (2018), 895-906, doi.10.1080/1064119X.2017.1397068.
5. Arish, N., "Electromagnetic performace analysis of linear vernier machine with PM and HTS-Bulk", ***Physica C: Superconductivity and its Applications,*** Vol. 579, (2020). doi.org/10.1016/j.physc.2020.1353751.
6. Li, D., Qu, R and Lipo, TA., " High-Power-Factor Vernier Permanent-Magnet Machines", ***IEEE Transactions on Industry Applications,*** Vol. 50, No. 6, (2013). doi. 10.1109/TIA.2014.2315443.
7. Raihan, M.A.H., Baker, N., Smith, K andAlmoraya, A., "Linear consequent pole Halbach array flux reversal machine" ***TheJournal of Engineering,*** Vol. 2019, No. 17, (2019). doi. 10.1049/joe.2018.8110.
8. Shi, C., Qu, R., Gao, Y., Li, D., Jing, L and Zhou, Y. "Design and Analysis of an Interior Permanent Magnet Linear Vernier Machine" ***IEEE Transactions on Magnetics,*** Vol. 54, No. 11, (2018). doi.org/10.1109/TMAG.2018.2840832.
9. Almoraya, A.A., Baker, N.J., Smith, K.J., and Raihan, M.A.H., "Design and Analysis of a Flux-Concentrated Linear Vernier Hybrid Machine with Consequent Poles", ***IEEE Transactions on Industry Applications,*** Vol. 55, No. 5, (2019), 4595-4604. doi.org/10.1109/TIA.2019.2918499.
10. Huo, Y., Qu, R., Gao, Y., Jia, S and Fan, X., "Design of a linear vernier permanent magnet machine with high thrust force density and low thrust force ripple" IEEE International Electric Machines and Drives Conference, (2017). doi.10.1109/IEMDC.2017.8002234
11. Zhao, W., Zheng, J., Wang, J., Liu, G., Zhao, J. and Fang, Z., "Design and analysis of a linear permanent- magnet vernier machine with improved force density", ***IEEE Transactions Industrial Electronics,*** Vol. 63, No. 4, (2016), 2072–2082. doi.10.1109/TIE.2015.2499165
12. Shi, C., Li, D., Qu, R., Zhang, H., Gao, Y and Huo, Y., "A Novel Linear Permanent Magnet Vernier Machine with Consequent-Pole Permanent Magnets and Halbach Permanent Magnet Arrays" ***IEEE Transactions on Magnetics,*** Vol. 53, No. 11, (2017), 1-4. doi.10.1109/TIE.2015.2499165.
13. Nematsaberi, A. and Faiz, J., "A Novel Linear Stator-PM Vernier Machine With Spoke- Type Magnets", ***IEEE Transactions on Magnetics***, Vol. 54, No. 11, (2018), 1–5. doi.org/10.1109/iraniancee.2019.878640.
14. Arish, N., Teymoori, V., Yaghobi, H. and Moradi, M., " Design of New Linear Vernier Machine with Skew and Halbach Permanent Magnet for Wave Energy Converter", 34 th P ower System Conference (PSC), (2019). doi.10.1109/PSC49016.2019.9081549.
15. Arish, N and Teymoori, V., "Development of Linear Vernier Hybrid Permanent Magnet Machine for Wave Energy Converter" ***International Journal of Engineering, Transaction B:*** **Applications,** Vol. 33, No. 5, (2020), 805-813. doi.org/10.5829/ije.2020.33.05b.12.
16. Khaliq, S., Zhao, F and Kwon, B., "Design and analysis of a dual stator spoke type linear vernier machine for wave energy extraction," IEEE International Magnetics Conference (INTERMAG), Beijing, (2015), doi.10.1109/INTMAG.2015.7157480.
17. Ardestani, M., Arish, N. and Yaghobi, H., "A new HTS dual stator linear permanent magnet Vernier machine with Halbach array for wave energy conversion", ***Physica C:***

Superconductivity and its Applications, Vol. 567, (2020). doi.10.1016/j.physc.2019.1353593.

18. Almoraya, A.A., Baker, N.J., Smith, K.J and Raihan, M.A.H.: "Development of a double-sided consequent pole linear vernier hybrid permanent-magnet machine for wave energy converters", in '2017 IEEE International Electric Machines and Drives Conference, IEMDC 2017' (2017). doi:10.1109/IEMDC.2017.8002157.
19. Zhao, W., Liu, X., Chau, K.T., Xiao, F., Cheng, M and Du, Y.: 'Linear primary permanent magnet vernier machine for wave energy conversion*'IET Electric Power Applications*, Vol. 9, No. 3, (2015). doi.org/10.1049/iet-epa.2014.0138 .
20. Almoraya, A.A., Baker, N.J., Smith, K.J and Raihan, M.A.H, "An investigation of a linear flux switching machine with tapered ferromagnetic poles", in '2017 20th International Conference on Electrical Machines and Systems, ICEMS 2017' (2017) doi.org/10.1109/ICEMS.2017.8056083.
21. Baker, N.J., Raihan, M.A.H., Almoraya, A.A., Burchell, J.W., Mueller, M.A., "Evaluating Alternative Linear Vernier Hybrid Machine Topologies for Integration into Wave Energy Converters" ***IEEE Transactions on Energy Conversion***, Vol. 33, No. 4 (2018). doi.org/10.1109/TEC.2018.2873913.
22. Rostami, M., Nadery, P and Shiri, A., " Analysis of Linear Primary Permanent Magnet Vernier Machine Using Finite element method" in '2020 11th Power Electronics, Drive Systems, and Technologies Conference, PEDSTC 2020' (2020). doi: 10.1109/PEDSTC49159.2020.9088394.
23. Arish, N., Ardestani, M., and Hekmati, A., " Study on the optimum structure of the rotor slot shape for a 20-kW HTS", ***Physica C: Superconductivity and its Applications,*** Vol. 567, No. 12, (2020).
24. Movahedi, A., Kavianpour, M and Yamini, O., "Experimental and Numerical Analysis of the Scour Profile Downstream of Flip Bucket with Change in Bed Material Size." ***ISH Journal of Hydraulic Engineering***, Vol. 25, No. 8, (2019), doi.10.1080/09715010.2017.1398111.
25. A. N. Patel and B. N. Suthar, "Cogging torque reduction of sandwiched stator axial flux permanent magnet brushless dc motor using magnet notching technique", ***International Journal of Engineering Transaction A: Basics***, Vol. 32, No. 7, (2019), 940-946. doi.10.5829/ije.2019.32.07a.06.
26. Botha, C.D., Kamper, M.J., Wang, R.-J., Sorgdrager, A.J., "Force Ripple and Cogging Force Minimisation Criteria of Single-Sided Consequent-Pole Linear Vernier Hybrid Machines", (2020), 469-475, doi: 10.1109/ICEM49940.2020.9270845.
27. Sorgdrager, A.J., Wang, R.J., Grobler, A.J "Robust Torque Ripple Mitigation of a Line-Start PMSM by Means of the Taguchi Method," 2019 Southern African Universities Power Engineering Conference/Robotics and Mechatronics/Pattern Recognition Association of South Africa (SAUPEC/RobMech/PRASA), Bloemfontein, South Africa, 2019, 259-264, doi: 10.1109/RoboMech.2019.8704771.
28. Liu, Y., Zhu, Z.Q., " Influence of gear ratio on electromagnetic performance and geometries of Vernier permanent magnet synchronous machines", IEEE Energy Conversion Congress and Exposition, ECCE 2017. (2017). doi.org/10.1109/ECCE.2017.8096471.
29. Moradi Cheshmeh Beigi, H., "Design,. optimization and FEM analysis of a surface-mounted permanent-magnet brushless DC motor", ***International Journal of Engineering, Transaction B: Applications,*** Vol. 31, No. 2, (2018), 339-345. doi.10.5829/ije.2018.31.02b.19.
30. Arish, N., Ardestani, M., Teymoori, V., "Comparison of Dual Stator Consequent-pole Linear Permanent Magnet Vernier Machine with Toroidal and Concentrated Winding", in '2020 11th Power Electronics, Drive Systems, and Technologies Conference, PEDSTC 2020' (2020). doi: 10.1109/PEDSTC49159.2020.9088384.

Persian Abstract

چکیده

امروزه، اهمیت استفاده از ماشین های ورنیر در مبدلهای انرژی موج به دلیل ساختار ساده و توانایی آن در ایجاد نیروی رانش زیاد در سرعتهای پایین افزایش یافته است که به دلیل اثر دنده ای مغناطیسی است. ماشین خطی ورنیر با آهنربا دایمی در ساختار های مختلفی طراحی شده است. طراحی و انتخاب مناسب پارامترهای اصلی دستگاه باعث بهبود عملکرد و افزایش کارایی ماشین های ورنیر خطی می شود. یکی از این پارامترها شکل آهن ربا و نحوه جهت گیری مغناطیسی آنهاست. نوآوری این مقاله کاهش شار نشتی با تغییر شکل و تغییر جهتگیری مغناطیسی آهنرباهای دایمی است. به طوری که ، سه نوع ماشین خطی ورنیر با جهتگیری مغناطیسی و ساختار آهنربای مختلف از جمله V شکل ، آرایه هالباخ و قطب متعاقب ارائه شده است. ماشین های در نظر گرفته شده از نظر تراکم شار شکاف هوا ، EMF برگشتی ، شار PM ، اندوکتانس ، نیروی رانش ، نیروی بازدارندگی، تلفات، راندمان، ضریب قدرت، چگالی شار و خطوط شار با استفاده از روش المان محدود با نرم افزار مکسول تحت شرایط یکسان و حجم آهنربا یکسان با یکدیگر و ماشین موجود مقایسه شده اند. نتایج نشان میدهند که جهت گیری مغناطیسی و شکل آهن ربا های دایمی بر روی شار نشتی تاثیر قابل توجهی دارد و همه ی مدل های ارایه شده نسبت به مدل موجود شار نشتی کمتر و عملکرد بهتری دارند.